JACS
JOURNAL OF THE AMERICAN CHEMICAL SOCIETY
Article
Cite This: J. Am. Chem. Soc. 2018, 140, 11519−11525
pubs.acs.org/JACS

Toward Intrinsic Room-Temperature Ferromagnetism in Two-Dimensional Semiconductors

Chengxi Huang,[†] Junsheng Feng,[‡] Fang Wu,[§] Dildar Ahmed,[†] Bing Huang,[*,∥] Hongjun Xiang,[*,‡,⊥] Kaiming Deng,[†] and Erjun Kan[*,†]

[†]Department of Applied Physics and Institution of Energy and Microstructure, Nanjing University of Science and Technology, Nanjing, Jiangsu 210094, P.R. China

[‡]Key Laboratory of Computational Physical Sciences (Ministry of Education), State Key Laboratory of Surface Physics, and Department of Physics, Fudan University, Shanghai 200433, P.R. China

[§]School of Science, Nanjing Forestry University, Nanjing, Jiangsu 210037, P.R. China

[∥]Beijing Computational Science Research Center, Beijing 100193, P.R. China

[⊥]Collaborative Innovation Center of Advanced Microstructures, Nanjing 210093, P.R. China

Supporting Information

ABSTRACT: Two-dimensional (2D) ferromagnetic semiconductors have been recognized as the cornerstone for next-generation electric devices, but the development is highly limited by the weak ferromagnetic coupling and low Curie temperature (T_C). Here, we reported a general mechanism which can significantly enhance the ferromagnetic coupling in 2D semiconductors without introducing carriers. On the basis of a double-orbital model, we revealed that the superexchange-driven ferromagnetism is closely related to the virtual exchange gap, and lowering this gap by isovalent alloying can significantly enhance the ferromagnetic (FM) coupling. On the basis of the experimentally available two-dimensional CrI_3 and $CrGeTe_3$, the FM coupling in two semiconducting alloy compounds $CrWI_6$ and $CrWGe_2Te_6$ monolayers are calculated to be enhanced by 3∼5 times without introducing any carriers. Furthermore, a room-temperature ferromagnetic semiconductor is achieved under a small in-plane strain (4%). Thus, our findings not only deepen the understanding of FM semiconductors but also open a new door for realistic spintronics.

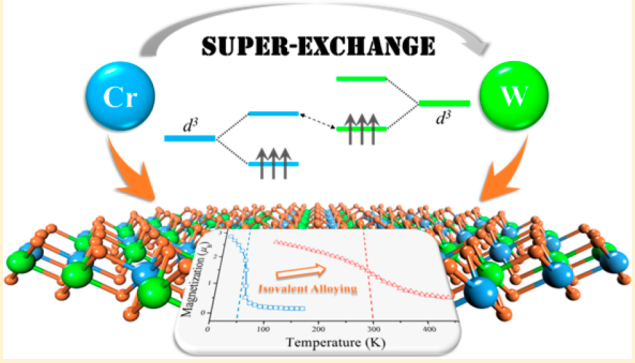

1. INTRODUCTION

The discovery of spintronic behaviors (e.g., giant magnetoresistance effect) gives new dimensions to manipulate the spin and charge of materials, leading to novel functional spintronic devices.[1] One of the most promising candidates of spintronic materials is ferromagnetic (FM) semiconductor. Different from the usual antiferromagnetic (AFM) insulators, FM semiconductors simultaneously possess spontaneous net magnetization and the moderate electrical resistivity at finite temperature, leading to potential spintronic applications such as data storage, sensing, capacitor, and logical devices.[2,3] For practical interests, a feasible FM semiconductor with strong ferromagnetism that can survive at room temperature (300 K) is highly desirable.[4] However, FM semiconductors are rare in nature and their Curie temperatures (T_C) are usually much lower than room temperature, such as the recent experimentally realized two-dimensional (2D) FM semiconductors whose T_C are below 45 K.[5−7] Actually, experimental observation of room-temperature intrinsic FM semiconductors has never been reported despite decades of tremendous efforts since the first FM semiconductor ($CrBr_3$)[8] was discovered more than half a century ago.

It is known that FM metals may have very high T_C (e.g., ∼420 K for Sr_2FeMoO_6 double perovskite[9] and ∼780 K for 2D Fe_2Si[10]) because of the strong double-exchange interaction driven by charge carriers.[11] Similarly, in the diluted magnetic semiconductors (DMSs), the carrier-mediated exchange could lead to a relatively strong FM coupling. However, the reproducible T_C is still limited below ∼200 K (e.g., 155 K for GaMnAs).[12−14] Carrier injection may further enhance the ferromagnetism,[15] but doping a high concentration of carriers may destroy the semiconducting properties. On the other hand, FM coupling driven by superexchange in a conventional intrinsic FM semiconductor is carrier-free, but is usually rather weak, resulting in a T_C below ∼100 K.[16−19] Although, in principle, the superexchange mechanism does not prohibit the occurrence of strong semiconducting ferromagnetism, it is still a critical and open question as to whether the T_C of an intrinsic

Received: July 25, 2018
Published: August 21, 2018

DOI: 10.1021/jacs.8b07879
J. Am. Chem. Soc. 2018, 140, 11519−11525

FM semiconductor can be improved up to room temperature without introducing carriers?

Here, we demonstrate that superexchange indeed can lead to carrier-free room-temperature semiconducting ferromagnetism. Using a double-orbital model, we reveal a general mechanism that FM coupling in a semiconductor can be significantly enhanced by reducing the virtual exchange gap (G_{ex}) between the occupied and empty spin-polarized orbitals of adjacent magnetic ions. The explored mechanism is then applied to two experimentally reported systems, namely, CrI_3 and $CrGeTe_3$ thin layers, which are intrinsic FM semiconductors with low T_C.[5,6] By isovalent alloying of Cr with W to construct alloy compounds $CrWI_6$ and $CrWGe_2Te_6$ monolayers, the G_{ex} between occupied W-$t_{2g}\uparrow$ and empty Cr-$e_g\uparrow$ orbitals is much reduced. First-principles calculations and classical Monte Carlo (MC) simulations demonstrated that both $CrWI_6$ and $CrWGe_2Te_6$ monolayers are robust intrinsic FM semiconductors with T_C of ∼180 K, which is indeed much higher than that of the pristine CrI_3 (45 K) and $CrGeTe_3$ thin layers (30 K). And the T_C of $CrWGe_2Te_6$ monolayer can be enhanced up to room temperature (300 K) under a small tensile strain (4%) without introducing any carriers. Besides, the applicability of the proposed mechanism is also confirmed in another typical magnetic system, that is, the $HgCr_2S_4$ spinel and MnS_2 monolayer.

2. METHODS

Our first-principles calculations were based on density functional theory (DFT) implemented in the Vienna Ab Initio Simulation Package (VASP).[20] Generalized gradient approximation (GGA) for exchange-correlation functional given by Perdew, Burke, and Ernzerhof (PBE)[21] was used. The effective Hubbard U_{eff} = 3 and 1 eV were added according to Dudarev's[22] method for the Cr-d and W-d orbitals, respectively. Because the U_{eff} values of Cr in different systems are usually taken within the range of 2∼4 eV and the U_{eff} difference of 2 eV between 3d and 5d elements ($U_{eff,3d} - U_{eff,5d}$ = 2 eV) is reasonable.[23−25] A test for different U_{eff} values is also performed (Table S2 in the Supporting Information). The projector augmented wave (PAW)[26] method was used to treat the core electrons. We also have performed calculations using HSE06 hybridized functional[27] on the magnetic properties. The results are very similar to those from DFT+U calculations (Table S4 in the Supporting Information). The plane wave cutoff energy was set to be 500 eV and the first Brillouin zone was sampled by using a Γ-centered 12 × 12 × 1 Monkhorst−Pack[28] grid. A vacuum space of 20 Å along the z direction was adopted to model the 2D system. The spin−orbit coupling (SOC) was included in the electronic self-consistent calculations. The phonon calculations were performed by using the PHONOPY code.[29] The first-principles-based cluster expansion[30] (CE) calculations and Monte Carlo (MC) simulations for the ordered−disordered phase transition of alloy systems are performed by using the Alloy-Theoretic Automated Toolkit (ATAT) package.[31] To confirm the stability of the $CrWI_6$ and $CrWGe_2Te_6$, we adopt our global optimization approach[32] for searching quasi-2D structures as implemented in the Crystal structure Analysis by Particle Swarm Optimization (CALYPSO) code.[33,34] In these calculations, the only given prior structure information is the chemical composition.

The spin dynamical process is studied by the classical Metropolis MC simulations.[35] For CrI_3, $CrWI_6$, and $CrWGe_2Te_6$ monolayer, a 30 × 30 2D honeycomb spin−lattice containing 1800 spin sites with the periodic boundary condition is used. During the simulation steps, each spin is rotated randomly in all directions. The average magnetization per site is taken after the system reaches the equilibrium (with at least 10^5 simulation steps) state at a given temperature. The Curie temperature (T_C) is taken as the critical point of the specific heat, defined as $C_V = (\langle E^2\rangle - \langle E\rangle^2)/k_BT$.[2] The estimated T_C of CrI_3 monolayer (∼50 K) is very close to the experimental result (∼45 K), suggesting the rationality of this method.

3. RESULTS AND DISCUSSION

3.1. Weak Ferromagnetism in CrI_3 and $CrGeTe_3$. To explore how to enhance the ferromagnetism, first of all, it is necessary to understand why the ferromagnetism is usually so weak in an intrinsic FM semiconductor. The recent experimentally reported 2D intrinsic FM semiconductors, namely, the CrI_3[6] and $CrGeTe_3$,[5] are two typical examples. In both systems, each Cr is coordinated by six ligands (I or Te) (Figure 1a,b). Because of the octahedral crystal field, the Cr-d

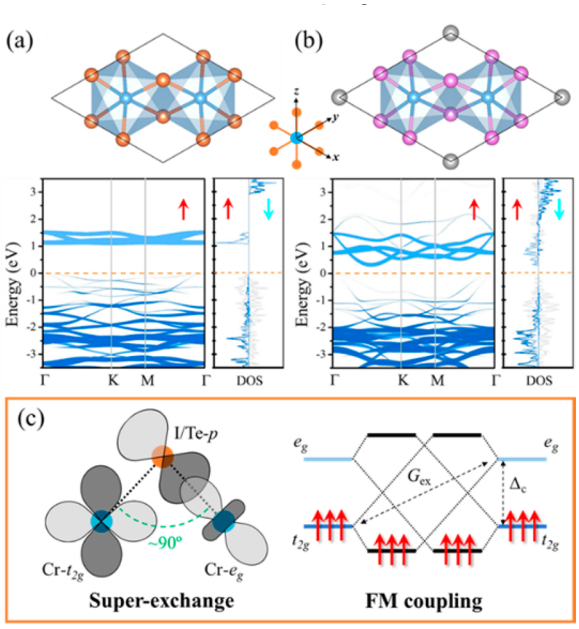

Figure 1. Atomic structure (top view), projected band structure, and density of states (DOS) for Cr-t_{2g} (dark blue), Cr-e_g (light blue), I-p (gray), and Te-p (gray) orbitals of (a) CrI_3 and (b) $CrGeTe_3$ monolayer. Blue, orange, pink, and gray balls represent Cr, I, Te, and Ge atoms, respectively. Red and cyan arrows represent spin-up and spin-down channels. (c) Schematic diagrams of the superexchange interaction and FM coupling in CrI_3 and $CrGeTe_3$ monolayer. G_{ex} is the virtual exchange gap. Δ_c represents the energy gap opened by the crystal field. Red arrows represent the spin-up electrons.

orbitals split into two parts, that is, the threefold t_{2g} and twofold e_g manifolds. The lower t_{2g} orbitals are half occupied while the higher e_g orbitals are empty, which makes these systems magnetic semiconducting (Figure 1a,b). Furthermore, in both systems, the Cr−I/Te−Cr bonding angle is close to 90°, which explains the occurrence of FM coupling according to the well-known Goodenough−Kanamori−Anderson (GKA)[36−38] rules of the superexchange theorem (Figure 1c). However, the overall FM coupling driven by superexchange is rather weak because of the competitive AFM interactions (i.e., the Cr−Cr direct exchange). But it is still unclear as to what is the higher limit of the strength of FM coupling in such systems. Can it be strong enough to survive at room temperature? If looking a little deeper into the electronic structures of CrI_3 and $CrGeTe_3$ monolayer, one may find a similarity between them, that is, the large energy gap between occupied $t_{2g}\uparrow$ and empty $e_g\uparrow$ orbitals. A reasonable doubt comes out that since the FM coupling originates from the

DOI: 10.1021/jacs.8b07879
J. Am. Chem. Soc. 2018, 140, 11519−11525

virtual exchange between a half occupied and an empty orbital (the $t_{2g}\uparrow$-p-$e_g\uparrow$ exchange in this case; see Figure 1c) in a superexchange system, if we can reduce the energy gap between them (i.e., the G_{ex}), will the FM coupling be enhanced?

3.2. Enhancing FM Coupling via Orbital Engineering. To explore how G_{ex} affects the magnetic coupling, here we introduce a double-orbital model from the perspective of the tight-binding theorem in which the lower orbital is half occupied and the higher one is empty. This is the simplest FM semiconducting system. On the basis of the mean field approximation, the general Hamiltonian is given as[39,40]

$$\hat{H} = \hat{H}_t + \hat{H}_M$$

where the first term H_t represents hopping between nearest neighboring sites and the second term H_M corresponds to the mean-field exchange field. To be more specific,

$$\hat{H}_t = \sum_{\mu\nu}\sum_{\sigma=\uparrow,\downarrow}(t_{i\mu j\nu,\sigma}c^{\dagger}_{i\mu,\sigma}c_{j\nu,\sigma} + h.c.)$$

$$\hat{H}_M = \sum_{l=i,j}\sum_{\sigma=\uparrow,\downarrow}\sum_{\mu=\alpha,\beta}\epsilon_{l\mu}c^{\dagger}_{l\mu\sigma}c_{l\mu\sigma} - \sum_{l=i,j}\sum_{\mu=\alpha,\beta}\frac{1}{2}u_l m_l \cdot S_{l\mu}$$

where i and j represent the two neighboring magnetic sites, μ and ν are the orbital indexes ($\mu, \nu = \alpha, \beta$), ϵ represents the on-site energy of each orbital, u_l represents the strength of exchange splitting, S is the spin operator, and m is the unit vector of the spin direction. The strength of crystal field is defined as $\Delta_{cl} = |\epsilon_{l\alpha} - \epsilon_{l\beta}|$. Generally speaking, in an intrinsic magnetic semiconductive system (e.g., transition-metal compound), Δ_{cl} for each cation is similar and $t_{i\mu j\nu} \ll u_l$ due to strong electronic correlation. For simplification, we assume that $\Delta_{ci} = \Delta_{cj} = \Delta_c$ and $t_{i\mu j\nu} = t$. In the usual case, $u_i = u_j = u$ and $\epsilon_{i\mu} = \epsilon_{j\mu}$, that is, $G_{ex} = \Delta_c$. When the second-order perturbation method is applied, the relative energies of FM (E_{FM}) and AFM (E_{AFM}) alignments are (see the Supporting Information for details)

$$E_{FM} = -\frac{2t^2}{G_{ex}}$$

$$E_{AFM} = -2t^2\left(\frac{1}{G_{ex} + u} + \frac{1}{u}\right)$$

From these equations, one finds that both E_{FM} and E_{AFM} decreases with the decreasing of G_{ex}. But as G_{ex} decreases, E_{FM} falls much more rapidly than E_{AFM} does when G_{ex} is approaching to near zero, leading to an increment of the total exchange energy ($E_{ex} = E_{AFM} - E_{FM}$) (Figure 2a).

Staggering the energy level between i and j sites is another possibility to reduce the G_{ex}. In this case, the $\alpha_i - \beta_j$ and $\alpha_j - \beta_i$ exchange are not equivalent. Such an energy level stagger can be realized by either introducing an exchange-split difference ($\Delta_u = u_i - u_j$) or average on-site energy difference ($\Delta_o = \epsilon_{i\alpha} - \epsilon_{j\alpha}$) between neighboring magnetic sites. We first consider the former case (i.e., $\Delta_u \neq 0$, while $\Delta_o = 0$. Here, we assume that $\Delta_u > 0$). It is easy to get $G_{ex} = \Delta_c - \Delta_u/2$. The relative energies are

$$E_{FM} = -t^2\left(\frac{1}{G_{ex}} - \frac{1}{G_{ex} - 2\Delta_c}\right)$$

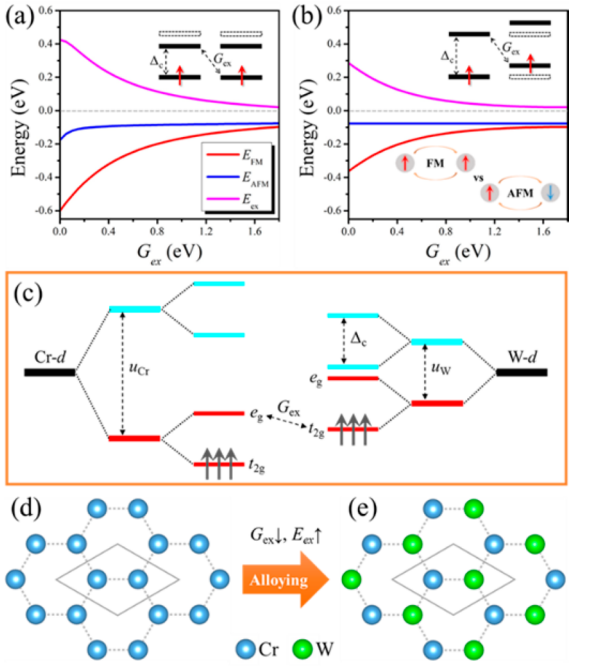

Figure 2. Relative energies of ferromagnetic (E_{FM}), antiferromagnetic (E_{AFM}) alignments and exchange energy ($E_{ex} = E_{AFM} - E_{FM}$) as a function of G_{ex} under the circumstance of (a) averagely lowering the higher empty orbitals and (b) staggering the energy levels between neighboring magnetic sites. (c) Schematic diagrams of orbital evolution and the origin of energy level staggering in Cr, W alloy systems. Red and cyan bars represent spin-up and spin-down orbitals, respectively. u_{Cr} and u_W are exchange splits for Cr- and W-d orbitals, respectively. Δ_c is the energy gap opened by the crystal field. (d) The pure phase and (e) one of the typical alloy phases for CrI_3- or $CrGeTe_3$-based systems.

$$E_{AFM} = -2t^2\left(\frac{1}{\Delta_c + u_0} + \frac{1}{u_0}\right)$$

where $u_0 = (u_i + u_j)/2$. One finds that E_{FM} increases along with G_{ex}, while E_{AFM} is independent of G_{ex} (Figure 2b). Thus, as G_{ex} decreases, E_{ex} also increases. For the case where the average on-site energies are different ($\Delta_o \neq 0$), the results are very similar (see the Supporting Information).

From the above analysis based on double-orbital model, we can deduce that the large G_{ex} of CrI_3 and $CrGeTe_3$ is probably responsible for their weak FM coupling. Once we can properly reduce the G_{ex} in these systems, their semiconducting ferromagnetism is expected to be greatly enhanced. Next, we will demonstrate this idea by first-principles calculations.

A practical way to reduce the G_{ex} and enhance semiconducting ferromagnetism is constructing alloyed transition-metal compounds. Because the exchange split and on-site energy of d orbitals for different transition metals under an octahedral field could be different. For instance, the tungsten (W) usually exhibits much smaller exchange split than Cr in an octahedral crystal field. This results in a distinct staggering between Cr-d and W-d orbitals, which may lead to reduction of G_{ex} between empty Cr-$e_g\uparrow$ and occupied W-$t_{2g}\uparrow$ orbitals (Figure 2c). The other reason that we choose W to alloying CrI_3 and $CrGeTe_3$ is that W can exhibit the same valence state (+3) and occupation state (d^3) as Cr in these systems. Note that although the W metal bulk is nonmagnetic, W has been widely used to synthesize alloys with strong magnetism, such as

DOI: 10.1021/jacs.8b07879
J. Am. Chem. Soc. 2018, 140, 11519−11525

the martensite.[41] To demonstrate our idea, here we focus on the case where the concentration of W is 50% (Figure 2d,e). The alloy compounds are denoted as $CrWI_6$ and $CrWGe_2Te_6$.

3.3. Stability and Feasibility of $CrWI_6$ and $CrWGe_2Te_6$. There could be plenty of possible alloyed configurations for $CrWI_6$ and $CrWGe_2Te_6$ depending on the distribution pattern of Cr and W at the metal sites. To find out the optimal alloyed configuration, we have considered six possible distribution patterns of Cr and W atoms in a 2 × 2 supercell containing four Cr and W sublattices (Figure 3a). We find that, for both

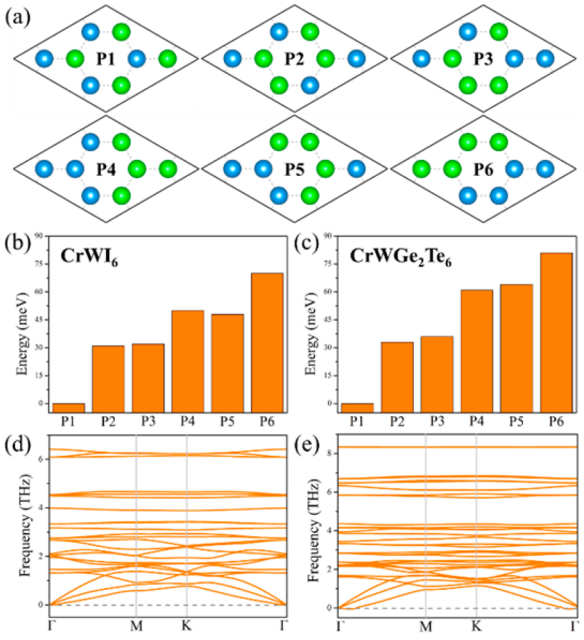

Figure 3. (a) Considered possible distribution patterns (P1−P6) of Cr and W atoms in a 2 × 2 supercell for $CrWI_6$ and $CrWGe_2Te_6$ monolayer. Blue and green balls represent Cr and W atoms, respectively. The I, Ge, and Te atoms are omitted for simplicity. Relative energies per formula unit for each considered distribution pattern of (b) $CrWI_6$ and (c) $CrWGe_2Te_6$ monolayer. Phonon dispersion for P1 pattern, namely, the honeycomb checkboard (d) $CrWI_6$ and (e) $CrWGe_2Te_6$ monolayer.

$CrWI_6$ and $CrWGe_2Te_6$, the honeycomb-checkboard (HC) pattern (see P1 in Figure 3a) is lower by at least 30 meV/formula-unit in energy compared to that of the other patterns. Note that the relative energies (Figure 3b) of different alloyed configurations are based on electronic energies. The enthalpy, zero-point energy, and site entropy are not considered in these calculations.

We further performed first-principles-based CE calculations to determine the intermediate alloy ground states. The results show that the ordered HC pattern is indeed the ground state for both $CrWI_6$ and $CrWGe_2Te_6$ (see the Supporting Information for details).

To examine the feasibility of HC $CrWI_6$ and $CrWGe_2Te_6$ monolayer, first, we calculated their formation energies (E_f). For $CrWI_6$, $E_f = (E_{CrWI6} - \mu_{Cr} - \mu_W - 6*\mu_I)/8$, and for $CrWGe_2Te_6$, $E_f = (E_{CrWGe2Te6} - \mu_{Cr} - \mu_W - 2*\mu_{Ge} - 6*\mu_{Te})/10$, where the chemical potential μ_{Cr}, μ_W, μ_I, μ_{Ge}, and μ_{Te} are taken from bcc Cr, W metal crystal, solid iodine, Ge crystal, and hexagonal Te crystal, respectively. The calculated E_f for HC $CrWI_6$ and $CrWGe_2Te_6$ monolayers are −0.474 and −0.216 eV, respectively, with negative values indicating exothermic chemical reaction. These values are comparable to those of pristine CrI_3 (−0.903 eV) and $CrGeTe_3$ (−0.552 eV) monolayer. From the CE results (Figure S3 in the Supporting Information), we can also find that the relative energies of the alloy phases are lower by ∼70 meV/metal compared to those of the pure phases, namely, CrI_3, WI_3, $CrGeTe_3$, and $WGeTe_3$. This indicates that the HC alloy phases can stably exist without any phase separation. To find out whether the HC configurations of $CrWI_6$ and $CrWGe_2Te_6$ are the globally stable structure, we also performed a global structural optimization based on our PSO algorithm for two-dimensional layered materials as implemented in the CALYPSO code. The results show that, among all predicted quasi-2D structures, the HC $CrWI_6$ and $CrWGe_2Te_6$ monolayers have the lowest energy.

Next, we calculated their phonon dispersion (Figure 3d,e) and performed ab initio molecular dynamical simulations (Figure S6 in the Supporting Information), which partially demonstrate their dynamical and thermal stabilities. To further consider the entropy effect and explore whether the ordered HC alloy phases can survive at a finite temperature, we performed MC simulations to explore the ordered−disordered phase transitions of the alloy systems (see the Supporting Information for details), in which the CE Hamiltonian used in MC simulations is fitted from the extensive first-principles total energy calculations. As shown in Figure 4a,b, it is interesting to

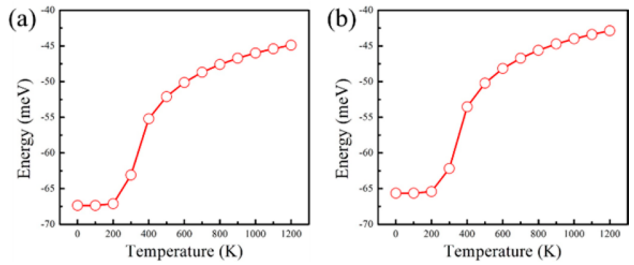

Figure 4. Excess energy as a function of temperature from Monte Carlo simulation for ordered−disordered phase transition of (a) $CrWI_6$ and (b) $CrWGe_2Te_6$ monolayer.

find that the ordered−disordered phase transition temperature for these two alloy systems are ∼400 K, which is sufficiently high for room-temperature applications.

3.4. Electronic and Magnetic Properties of $CrWI_6$ and $CrWGe_2Te_6$. In both $CrWI_6$ and $CrWGe_2Te_6$, W adopts the same oxidation (+3) and spin state ($S = {}^3/_2$) as Cr. Figure 5 (upper panel) shows the electron (−1 to 0 eV) and hole (0 to 1 eV) density around the Fermi level (set to 0 eV). One sees a distinct in-plane electron−hole separation. From the shape of the isosurfaces, we could consider that the electrons are mainly from W-t_{2g} orbitals while the holes are from Cr-e_g orbitals, indicating an energy level stagger between Cr-d and W-d orbitals near the Fermi level (Figure S7 in the Supporting Information). This is verified by the projected electronic structures (Figure 5, bottom panel). By extracting the maximally localized Wannier functions (MLWFs) (see the Supporting Information for details), we find that the energy level stagger is mainly caused by the exchange-split difference between Cr (u_{Cr} = ∼4.6 eV) and W (u_W = ∼1.8 eV). As a result, the G_{ex} between occupied W-$t_{2g}\uparrow$ and empty Cr-$e_g\uparrow$ orbitals (∼0.11 and ∼0.15 eV for $CrWI_6$ and $CrWGe_2Te_6$, respectively) in the alloy systems are much reduced compared

DOI: 10.1021/jacs.8b07879
J. Am. Chem. Soc. 2018, 140, 11519−11525

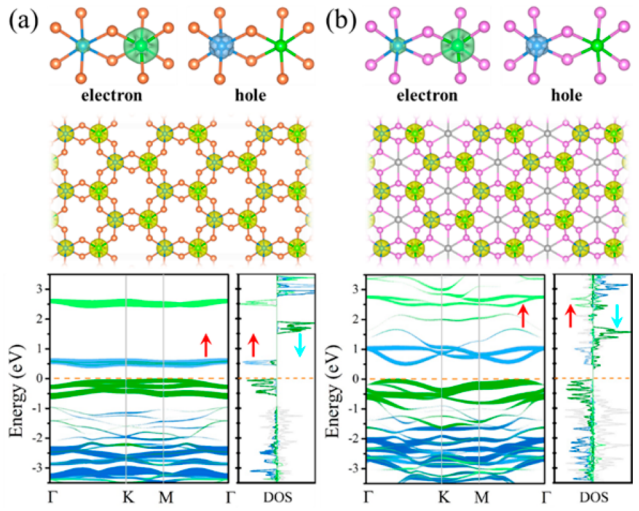

Figure 5. Spatial electron and hole density around the Fermi energy (upper panel), spin density (middle panel), projected band structures, and density of states (bottom panel) for (a) $CrWI_6$ and (b) $CrWGe_2Te_6$ monolayer. Blue, orange, pink, and gray balls represent Cr, I, Te, and Ge atoms, respectively. Dark blue, light blue, dark green, light green, and gray represent contribution from Cr-t_{2g}, Cr-e_g, W-t_{2g}, W-e_g, and I/Te-p orbitals, respectively. Red and cyan arrows represent spin-up and spin-down channels.

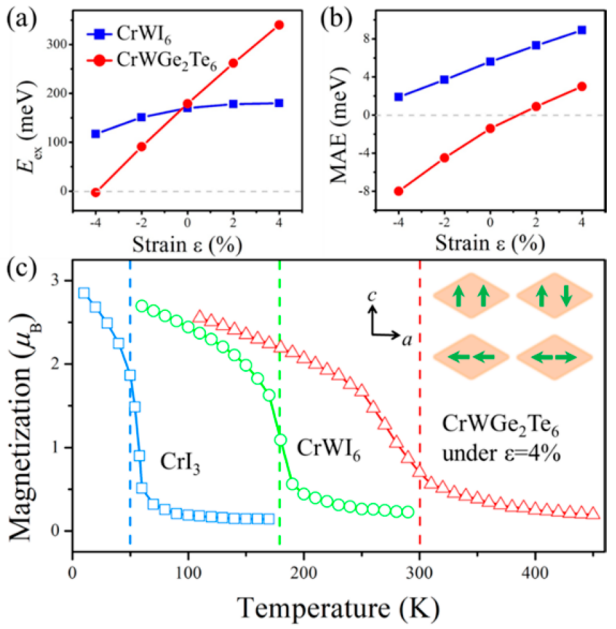

Figure 6. (a) Total exchange energy ($E_{ex} = E_{AFM} - E_{FM}$, positive values indicate ferromagnetic couplings) and (b) magnetic anisotropic energy (MAE = $E_{in\text{-}plane} - E_{out\text{-}of\text{-}plane}$, positive values indicate easy out-of-plane magnetization axis) per unit cell as a function of in-plane biaxial strain (ε). (c) Magnetic moment per site as a function of temperature for CrI_3, $CrWI_6$ monolayer, and $CrWGe_2Te_6$ monolayer under 4% tensile strain from Monte Carlo simulations. Inset: Four spin configurations considered in the DFT+SOC calculations.

to those between occupied Cr-t_{2g}↑ and empty Cr-e_g↑ orbitals (~2.0 and ~1.7 eV for CrI_3 and $CrGeTe_3$, respectively) in the pure hosts (Table S1 in the Supporting Information). As expected, our calculations show that the ground states of $CrWI_6$ and $CrWGe_2Te_6$ monolayer are FM with E_{ex} of 170 and 179 meV/unit cell, respectively, which are much larger than those of pristine CrI_3 (53 meV) and $CrGeTe_3$ (78 meV). Note that the enhancement of ferromagnetism in these systems is not mainly caused by the delocalization of W-d orbitals, which might strengthen the d-p-d hybridizations. In fact, our calculation shows that the hypothetical WI_3 monolayer is AFM instead of FM (see Table S1 and Figure S8 in the Supporting Information).

We also studied another key factor of the stability of long-range FM order in 2D systems, namely, the magnetocrystalline anisotropy.[42] Same as CrI_3, $CrWI_6$ monolayer exhibits an out-of-plane easy axis of net magnetization. Because of the enhanced spin−orbit coupling (SOC) effect of the 5d W^{3+} ion, the magnetocrystalline anisotropic energy (MAE = $E_{out\text{-}of\text{-}plane} - E_{in\text{-}plane}$) is 5.4 meV/unit cell (with respect to the in-plane hard axis), much larger than that of CrI_3 (1.5 meV/unit cell). But the $CrWGe_2Te_6$ monolayer exhibits an in-plane easy axis with MAE of −1.4 meV/unit cell, similar to 2D $CrGeTe_3$.[5]

It was reported that external strain can alter the magneto-crystalline anisotropy as well as the magnetic coupling;[43,44] here we also studied the strain effect on the ferromagnetism of $CrWI_6$ and $CrWGe_2Te_6$ monolayer. Figure 6a,b shows the E_{ex} and MAE as a function of the in-plane biaxial strain. We find that a tensile strain can only slightly increase the E_{ex} of $CrWI_6$. Interestingly, for $CrWGe_2Te_6$, E_{ex} is very sensitive to the strain. With a small tensile strain of 4%, the E_{ex} is nearly doubled (from 179 to 340 meV). Its global electronic band gap (0.4 eV) barely changes compared to the equilibrium state (0.41 eV). We also calculated its u, Δ_c, and G_{ex} under different strains (Table S1 in the Supporting Information). The results show that these parameters are slightly changed, which implies that the drastic change of E_{ex} with strain is probably due to the weakening of direct t_{2g}−t_{2g} AFM exchange. On the other hand, a tensile strain also greatly increases the MAE. For $CrWGe_2Te_6$, a tensile strain of 4% will change the orientation of easy axis from in-plane to out-of-plane and result in a MAE of 3.0 meV, which allows the formation of long-range FM order.

Now, we explore the magnetic behavior under finite temperatures and estimate the T_C. From the spin density (Figure 5 middle panel), one sees that the spin-polarized charges are mainly localized at each metal site; thus here we use the Heisenberg model in addition to a magnetic anisotropic term to describe the magnetic behavior of these systems (the in-plane anisotropy is omitted). The spin Hamiltonian

$$\hat{H} = -\sum_{\langle ij \rangle} J\vec{S_i}\cdot\vec{S_j} - \sum_{\langle i \rangle} D(S_{iz})^2$$

where the summation $\langle ij \rangle$ runs over all nearest-neighboring Cr and W sites. J is the exchange interaction parameter, D is the single-site magnetic anisotropy parameter, S_{iz} represent components of **S** along z (out-of-plane) orientations and $|\mathbf{S}| = {}^3/_2$ for both Cr and W. The calculated J and D from different spin configurations (Figure 6c) are listed in Table S3 in the Supporting Information. Then by classical Metropolis MC simulations (Figure 6c), the T_C of CrI_3, $CrWI_6$, and $CrWGe_2Te_6$ monolayer under a tensile strain of 4% are estimated to be ~50 K (very close to the experimental value ~45 K[6]), ~180 K, and ~ 300 K, respectively.

3.5. Generality. Finally, we briefly discuss the generality of the proposed mechanism, that is, reducing the G_{ex} to enhance

DOI: 10.1021/jacs.8b07879
J. Am. Chem. Soc. 2018, 140, 11519−11525

the semiconducting ferromagnetism. In particular, we consider the case of energy level staggering achieved by alloying transition-metal compounds which was already adopted experimentally to tune the properties in systems such as double perovskites. Here is a guideline to realize a desired FM alloy compound semiconductor with improved T_C: (i) choose a well-established magnetic semiconductor with transition-metal A as basis material; (ii) choose the transition-metal element B which should have the same occupation state (e.g., d^3) as A when embedded in the material; (iii) the Δ_u between A and B should be large enough to greatly reduce the G_{ex}. Thus, a 3d-4d or 3d-5d combination of A-B alloy compound is recommended. With this design principle, besides the two systems (CrI_3 and $CrGeTe_3$) presented here, we have found other systems (i.e., the $HgCr_2S_4$ bulk[45] and MnS_2 monolayer;[46] see the Supporting Information for details) whose ferromagnetism can also be enhanced by alloying engineering. Particularly, alloying Mn with Re in the MnS_2 monolayer will lead to a T_C of ∼340 K, exceeding the room temperature. Overall, we suggest that the proposed mechanism in this work can be widely applied in many magnetic systems (both 2D and 3D systems) to achieve high-temperature FM semiconductors.

4. CONCLUSION

In summary, based on a double-orbital model and first-principle calculations, we propose a new general idea to improve the T_C of a carrier-free FM semiconductor under the framework of superexchange theory. On the basis of recent experimentally realized FM thin layers, two feasible 2D alloy systems, namely, the $CrWI_6$ and $CrWGe_2Te_6$ monolayers, are used to prove our proposed mechanism. We show that reducing the G_{ex} will significantly enhance the FM coupling and improve the T_C up to room temperature. Thus, our results reveal new insights into the magnetic exchange and general mechanism of FM coupling in semiconductors, which gives great opportunity to realize room-temperature FM semiconductors. We expect future experimental realizations of room-temperature FM semiconductors in the alloy transition-metal compounds.

■ ASSOCIATED CONTENT

Supporting Information

The Supporting Information is available free of charge on the ACS Publications website at DOI: 10.1021/jacs.8b07879.

Double-orbital model analysis, detailed structural and electronic properties of $CrWI_6$ and $CrWGe_2Te_6$ monolayers, and magnetism in $HgCr_{2-x}Mo_xS_4$ and $Mn_xRe_{1-x}S_2$ bulk (PDF)

■ AUTHOR INFORMATION

Corresponding Authors

*ekan@njust.edu.cn
*hxiang@fudan.edu.cn
*bing.huang@csrc.ac.cn

ORCID

Chengxi Huang: 0000-0003-1491-3954
Erjun Kan: 0000-0003-0433-4190

Author Contributions

All authors have given approval to the final version of the manuscript.

Notes

The authors declare no competing financial interest.

■ ACKNOWLEDGMENTS

E.K. is supported by the NSFC (51522206, 11774173, 11474165, 11574151), NSF of Jiangsu Province (BK20130031), PAPD, the Fundamental Research Funds for the Central Universities (No. 30915011203), and New Century Excellent Talents in University (NCET-12-0628). Work at Fudan is supported by NSFC, the Special Funds for Major State Basic Research (2015CB921700), Program for Professor of Special Appointment (Eastern Scholar), Qing Nian Ba Jian Program. Work at CSRC is supported by the Science Challenge Project (No. TZ2016003) and NSAF U1530401. C.H. and E.K. acknowledge the support from the Tianjing Supercomputer Centre and Shanghai Supercomputer Center. We thank Shiqiao Du for help on cluster expansion calculations.

■ REFERENCES

(1) Fert, A. *Rev. Mod. Phys.* **2008**, *80*, 1517.
(2) Wolf, S. A.; Awschalom, D. D.; Buhrman, R. A.; Daughton, J. M.; von Molnár, S.; Roukes, M. L.; Chtchelkanova, A. Y.; Treger, D. M. *Science* **2001**, *294*, 1488−1495.
(3) Dietl, T. *Semicond. Sci. Technol.* **2002**, *17*, 377.
(4) Ando, K. *Science* **2006**, *312*, 1883−1885.
(5) Gong, C.; Li, L.; Li, Z.; Ji, H.; Stern, A.; Xia, Y.; Cao, T.; Bao, W.; Wang, C.; Wang, Y.; Qiu, Z. Q.; Cava, R. J.; Louie, S. G.; Xia, J.; Zhang, X. *Nature* **2017**, *546*, 265−269.
(6) Huang, B.; Clark, G.; Navarro-Moratalla, E.; Klein, D. R.; Cheng, R.; Seyler, K. L.; Zhong, D.; Schmidgall, E.; McGuire, M. A.; Cobden, D. H.; Yao, W.; Xiao, D.; Jarillo-Herrero, P.; Xu, X. *Nature* **2017**, *546*, 270−273.
(7) Li, B.; Xing, T.; Zhong, M.; Huang, L.; Lei, N.; Zhang, J.; Li, J.; Wei, Z. *Nat. Commun.* **2017**, *8*, 1958.
(8) Tsubokawa, I. *J. Phys. Soc. Jpn.* **1960**, *15*, 1664−1668.
(9) Kobayashi, K.-I.; Kimura, T.; Sawada, H.; Terakura, K.; Tokura, Y. *Nature* **1998**, *395*, 677−680.
(10) Sun, Y.; Zhuo, Z.; Wu, X.; Yang, J. *Nano Lett.* **2017**, *17*, 2771−2777.
(11) Zener, C. *Phys. Rev.* **1951**, *82*, 403.
(12) Ohno, H. *Science* **1998**, *281*, 951−956.
(13) Dietl, T. *Nat. Mater.* **2010**, *9*, 965−974.
(14) Dietl, T.; Ohno, H. *Rev. Mod. Phys.* **2014**, *86*, 187.
(15) Zhou, J.; Sun, Q. *Nanoscale* **2014**, *6*, 328.
(16) Matthias, B. T.; Bozorth, R. M.; Van Vleck, J. H. *Phys. Rev. Lett.* **1961**, *7*, 160.
(17) Baltzer, P. K.; Lehmann, H. W.; Robbins, M. *Phys. Rev. Lett.* **1965**, *15*, 493.
(18) Kimura, T.; Kawamoto, S.; Yamada, I.; Azuma, M.; Takano, M.; Tokura, Y. *Phys. Rev. B: Condens. Matter Mater. Phys.* **2003**, *67*, 180401.
(19) Huang, C.; Du, Y.; Wu, H.; Xiang, H.; Deng, K.; Kan, E. *Phys. Rev. Lett.* **2018**, *120*, 147601.
(20) Kresse, G.; Hafner, J. *Phys. Rev. B: Condens. Matter Mater. Phys.* **1993**, *47*, 558.
(21) Perdew, J. P.; Burke, K.; Ernzerhof, M. *Phys. Rev. Lett.* **1996**, *77*, 3865.
(22) Dudarev, S. L.; Botton, G. A.; Savrasov, S. Y.; Humphreys, C. J.; Sutton, A. P. *Phys. Rev. B: Condens. Matter Mater. Phys.* **1998**, *57*, 1505.
(23) Solovyev, I. V.; Dederichs, P. H.; Anisimov, V. I. *Phys. Rev. B: Condens. Matter Mater. Phys.* **1994**, *50*, 16861.
(24) Wang, L.; Maxisch, T.; Ceder, G. *Phys. Rev. B: Condens. Matter Mater. Phys.* **2006**, *73*, 195107.
(25) Giovannetti, G.; Capone, M. *Phys. Rev. B: Condens. Matter Mater. Phys.* **2014**, *90*, 195113.

(26) Blöchl, P. E. *Phys. Rev. B: Condens. Matter Mater. Phys.* **1994**, *50*, 17953.
(27) Krukau, A. V.; Vydrov, O. A.; Izmaylov, A. F.; Scuseria, G. E. *J. Chem. Phys.* **2006**, *125*, 224106−224110.
(28) Monkhorst, H. J.; Pack, J. D. *Phys. Rev. B* **1976**, *13*, 5188.
(29) Togo, A.; Tanaka, I. *Scr. Mater.* **2015**, *108*, 1−5.
(30) Connolly, J. W. D.; Williams, A. R. *Phys. Rev. B: Condens. Matter Mater. Phys.* **1983**, *27*, 5169.
(31) van de Walle, A.; Asta, M.; Ceder, G. *CALPHAD: Comput. Coupling Phase Diagrams Thermochem.* **2002**, *26*, 539−553.
(32) Luo, W.; Ma, Y.; Gong, X.; Xiang, H. *J. Am. Chem. Soc.* **2014**, *136*, 15992−15997.
(33) Wang, Y.; Lv, J.; Zhu, L.; Ma, Y. *Phys. Rev. B: Condens. Matter Mater. Phys.* **2010**, *82*, 094116.
(34) Wang, Y.; Lv, J.; Zhu, L.; Ma, Y. *Comput. Phys. Commun.* **2012**, *183*, 2063−2070.
(35) Wang, P.; Ren, W.; Bellaiche, L.; Xiang, H. *Phys. Rev. Lett.* **2015**, *114*, 147204.
(36) Anderson, P. W. *Phys. Rev.* **1950**, *79*, 350.
(37) Goodenough, J. B. *Phys. Rev.* **1955**, *100*, 564.
(38) Kanamori, J. *J. Phys. Chem. Solids* **1959**, *10*, 87−98.
(39) Katsura, H.; Nagaosa, N.; Balatsky, A. V. *Phys. Rev. Lett.* **2005**, *95*, 057205.
(40) Qiao, Z.; Jiang, H.; Li, X.; Yao, Y.; Niu, Q. *Phys. Rev. B: Condens. Matter Mater. Phys.* **2012**, *85*, 115439.
(41) Hajra, R. N.; Rai, A. K.; Tripathy, H. P.; Raju, S.; Saroja, S. *J. Alloys Compd.* **2016**, *689*, 829−836.
(42) Mermin, N. D.; Wagner, H. *Phys. Rev. Lett.* **1966**, *17*, 1133.
(43) Ingle, N. J. C.; Elfimov, I. S. *Phys. Rev. B: Condens. Matter Mater. Phys.* **2008**, *77*, 121202.
(44) Li, X.; Yang, J. *J. Mater. Chem. C* **2014**, *2*, 7071−7076.
(45) Hastings, J. M.; Corliss, L. M. *J. Phys. Chem. Solids* **1968**, *29*, 9.
(46) Kan, M.; Adhikari, S.; Sun, Q. *Phys. Chem. Chem. Phys.* **2014**, *16*, 4990−4994.

DOI: 10.1021/jacs.8b07879
J. Am. Chem. Soc. 2018, 140, 11519−11525